# A Ka-band Satellite Beacon Receiver for Propagation Experiment

Andrej Hrovat[1], Gorazd Kandus[1], Urban Kuhar[1,2], Arsim Kelmendi[1,2], Andrej Vilhar[1]

[1]Jozef Stefan Institute, Department of Communication Systems, Ljubljana, Slovenia
[2]Jozef Stefan International Postgraduate School, Ljubljana, Slovenia

**Abstract:** The design of a low-cost beacon receiver based on software defined radio is presented. The motivation for such a receiver is to investigate atmospheric impairments at the Ka frequency band. The receiver has been tested by the Hotbird 13A, ASTRA 3B and Alphasat satellite beacon signals. A GNU Radio software development toolkit and a USRP device were used for the development of a beacon receiver application. We have tested and validated the beacon receiver operation by the linearity test, by comparing the received signal levels with the corresponding rainfall data, and by comparing the measurement results with the appropriate ITU-R models. The low-cost beacon receiver passed all these tests successfully, confirming that we established a reliable measuring system. After the validation period we were monitoring the measured data on a daily basis, excluding erroneous data and regularly implementing system improvements. The validated data was further processed by a MATLAB tool where statistical analysis is performed. In particular, we developed procedures for attenuation and scintillation analysis as well as procedures for the analysis of second order statistics, corresponding to the fade duration and fade slope distribution. Measurement data processing was performed in three phases, each phase giving predefined output results. These results range from raw propagation data via intermediate propagation data and analysed experimental statistics up to the graphical statistical representation.

**Keywords:** satellite signal propagation; Ka-band; beacon measurements; software defined radio

# Satelitski sprejemnik v Ka frekvenčnem pasu za preizkus razširjanja radijskih valov

**Izvleček:** V članku je predstavljen načrt nizko cenovnega sprejemnika satelitskega svetilniškega signala na osnovi programirljivega radia. Sprejemnik je namenjen raziskavam vpliva vremena na sprejem signala v Ka frekvenčnem pasu. Testirali smo ga s signali iz satelitov Hotbird 13A, ASTRA 3B in Alphasat. Pri razvoju sprejemnika smo uporabili programsko razvojno orodje GNU Radio in USRP napravo. Delovanje sprejemnika smo preizkusili in ocenili s pomočjo testa linearnosti. Nivo satelitskega signala smo primerjali z ustreznimi podatki o padavinah, poleg tega pa smo izmerjene vrednosti primerjali tudi z izračuni na osnovi ITU-R modelov. Nizkocenovni sprejemnik je uspešno prestal vse teste, kar potrjuje, da je primeren za izvajanje meritev svetilniških satelitskih signalov. Z njim smo dnevno pregledovali izmerjene podatke, izključevali napačne podatke in stalno izboljševali sistem. Preverjene podatke smo nato obdelali z orodjem MATLAB in izvedli statistično analizo. Razvili smo postopke za analizo slabljenja in migljanja ter postopke za statistično analizo drugega reda ob upoštevanju trajanja in hitrosti spreminjanja presiha. Obdelavo izmerjenih podatkov smo izvajali v treh fazah tako, da smo v vsaki fazi dobili rezultate v predpisani obliki. Ti rezultati obsegajo osnovne podatke o razširjanju radijskih valov, statistično analizo meritev in tudi njihovo grafično predstavitev.

**Ključne besede:** razširjanje satelitskega signala; Ka-pas; meritve svetilnika; programirljivi radio

* Corresponding Author's e-mail: andrej.hrovat@ijs.si

## 1 Introduction

Satellite is the only viable means of providing connectivity that can reach anybody nearly anywhere. In the middle of the ocean, on an airplane in the sky or in a small village, satellite can ensure ubiquitous access and coverage on a global scale.

As the satellite transmissions at frequencies below 15 GHz are becoming congested, it is necessary to use higher frequency bands to provide wide range of broadband communication services. However, signal transmission at Ka and Q/V bands is more sensitive to atmospheric impairments, especially to attenuation due to rain, which severely affect link availability [1].

Real-time estimation and possibly short-term prediction of such impairments can be helpful. In order to enable the design of advanced fade mitigation techniques over a wide satellite coverage area, a satellite channel modelling is required. For improved accuracy and geographical expansion of the models, a coordinated set of measurements is required on a wide scale, comprising several measurement locations. To achieve this goal, several Ka/Q-band (20/40 GHz) beacon receivers have been developed and installed across Europe to receive the signal from the Alphasat Aldo Paraboni TDP#5 payload, mostly encouraged by ESA and COST Action IC0802 [2, 3, 4].

Four Ka-band beacon receivers, based on SDR (Software Defined Radio) technology, as has been the practice in a few other similar experiments [5, 6, 7], were installed recently in Ljubljana, Lisec, Graz and Krvavec in the scope of ESA PECS project SatProSi which results are presented in this paper. In June 2012 we started with the measurements of the 19.7 GHz beacon from the Eutelsat Hotbird 13A, formerly known as Hotbird 6, at the JSI site in Ljubljana. In July 2013 we switched to the ASTRA 3B satellite, which transmits the beacon at the carrier frequency of 20.2 GHz. In August 2013 we installed the second receiver on Lisec, Slovenia, also receiving the beacon from the ASTRA 3B satellite. Finally, in February 2014 we installed the third receiver at the Hilmwarte site in Graz, Austria, and started with measurements of the Alphasat beacon at 19.7 GHz. The measurement network was additionally extended after the project completion, in February 2015. At Krvavec, Slovenia, another ASTRA 3B beacon receiver was installed.

At the level of software design, actions are being taken towards the development of a common data processing tool. At COST Action IC0802 several such tools, dealing with propagation measurements and modelling for the design of prediction and impairment mitigation techniques have been presented. The goal of such tool is to design procedures for processing the measured data, thus increasing the reliability of obtained statistical data, while remaining its usage user friendly, possibly by increasing the application of standalone automatic procedures. With the motivation to make the procedures standardized, thus achieving comparability of obtained results, the activities are being further upgraded and extended within the Group of the AlphaSat Aldo Paraboni propagation Experimenters (ASAPE) [8].

In this paper, the design and development of a SDR satellite beacon receiver is described. The beacon receiver operation was tested and validated by the linearity test, by comparing the received signal levels with the corresponding rainfall data, and by comparing the measurement results with the appropriate ITU-R models.

## 2 Beacon receiver

Beacon receiver, developed at Jozef Stefan Institute, is based on the Software Defined Radio (SDR) platform. USRP platform in combination with GNU Radio software framework was chosen. The measurements are collected on a PC and stored in the cloud storage. This approach is both flexible and low-cost. The receiver was improved gradually until satisfying and reliable performance was reached.

The following requirements have been defined for the beacon receiver design:
-    tracking capability of the signal in the case of frequency drift,
-    capability of signal reacquisition after temporal loss of signal during deep fades,
-    sampling rate high enough for adequate scintillation tracking,
-    robustness, high reliability and long-term operation with minimal or no periods of interruption.

The basic block scheme of the beacon receiver is depicted in Figure 1. The received signal is fed to Low Noise Block (LNB) which down-converts the signal to the IF (Intermediate Frequency) at L-band. Signal is then lead through coaxial cable to USRP, equipped with DBSRX2 daughterboard, where it is further down-converted, sampled and sent to a PC over Ethernet. DB-SRX2 daughterboard ensures that signal is sent to the baseband and filtered before sampling to avoid aliasing. Signal is quadrature-sampled with 400 kHz sample rate and resolution of 14 bits. On PC, Ubuntu Linux and GNU Radio are installed.
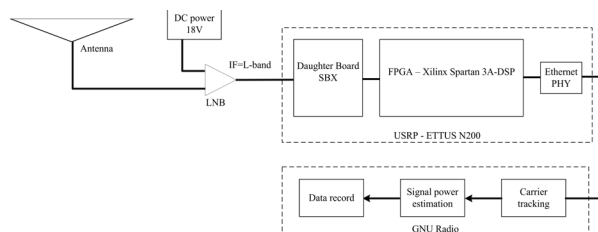


**Figure 1:** Beacon receiver for signal measurement

### 2.1 Hardware design

Based on available literature, market analysis and experience, the following hardware configuration was chosen for satellite ground station:
-    outdoor unit composed of Ka-band receive only antenna system - Prodelin 3120 Series and LNB Norsat 9000HB-2,
-    indoor unit composed of USRP N200/N210 box with the DBSRX2 daughterboard and

- control PC (Ubuntu linux OS, GNU radio framework) running signal processing and data logging.

### 2.1.1 Antenna and low noise block

The beacon receiver chain begins with an offset dish antenna manufactured by Prodelin [9]. The antenna measures 1.2 m in diameter and provides a gain of 45.8dBi at 19.701 GHz (Ka-band). It is mounted on a weighted iron stand, vertically to the floor. Figure 2 shows one of the receiver stations located at the Jozef Stefan Institute in Ljubljana.



a)



b)

**Figure 2:** 1.2m antenna (a) and LNB with feed (b)

In antennas focal point, an aluminium corrugated horn is mounted as a signal receptor which is connected to the LNB (shown in Figure 2 b). Since the feed's output is round waveguide the waveguide shape converter to LNB WR42 coverage flange is used. The LNB 9000HB-2, manufactured by NORSAT [10], with a frequency range of 19.2–20.2 GHz filters, amplifies and down coverts the received signal. Its block scheme is shown in Figure 3.
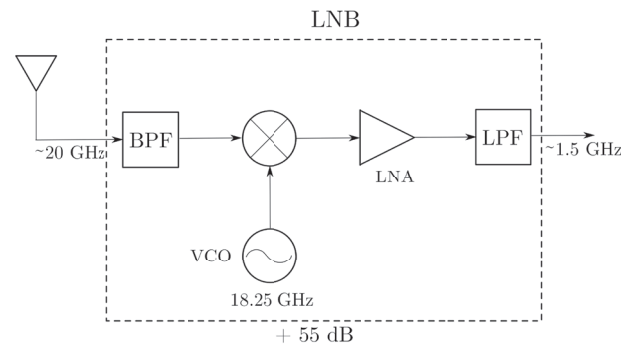


**Figure 3:** LNB configuration

The signal carrier at about 20 GHz is filtered in order to remove the mirror frequency and mixed with LNB's local oscillator (LO) which is locked at 18.25 GHz. Next, it is filtered to cut off signal sum and other harmonics. Finally, the signal is amplified with low noise amplifier (LNA) and filtered again to increase the carrier to noise ratio (CNR). The total gain provided by LNB is 55 dB and its noise Figure is 1.4 dB. The LNB's output 50 Ω N-type connector is joined to the indoor unit by a coaxial cable. In addition, through the coaxial cable also an 18 V DC voltage is supplied to the LNB.

### 2.1.2 Universal Software Radio Peripheral

The indoor unit is composed of the Universal Software Radio Peripheral (USRP) which is a range of software-defined radios manufactured by Ettus [11], now a member of the National Instruments group, and personal computer running Ubuntu linux and GNU Radio for data acquisition and logging software. In particular, the Networked series model (N200/N210) is installed in the receiver chain and controlled by GNU Radio framework [12]. An USRP includes motherboard which contains ADC, DAC and FPGA with connection to the Ethernet bus. It supports different daughterboards which are used as RF front-ends and can operate as receivers, transmitters or transcievers, depending on the model.

The USRP N210 series motherboard contains Xilinx FPGA, 100 MS/s dual analog to digital converter (ADC), 400 MS/s dual digital to analog converter (DAC) and an Ethernet interface. Motherboard gets pre-processed signal from DBSRX2 daughterboard and samples it with dual ADC. Samples are sent to computer over Ethernet.

For the RF front-end USRP DBSRX2 [11] daughterboard is used. It contains a programmable filter with a range up to 60 MHz, a mixer and a low noise amplifier. It can operate at frequencies between 800 - 2300 MHz. The block scheme of DBSRX2 is shown in Figure 4. Additionally, DBSRX2 also supplies LNB with 18 DC voltage.
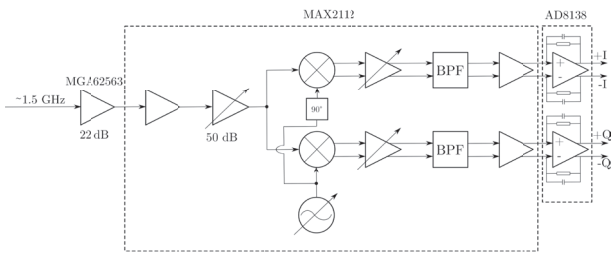
**Figure 4:** Daughterboard DBSRX2 block scheme

## 2.2 Signal processing

Software development was performed in GNURadio. It is an open-source framework with digital signal processing blocks which works with different types of data streams processed by signal processing blocks. Signal processing blocks are written in C++ or in Python, and connected by Python script.

Figure 5 depicts receiver high level software architecture. Signal samples received on ethernet bus are exposed to GNURadio via USRP Source block. Samples in the form of stream of complex numbers are sent to high pass filter (HPF) where unwanted DC spurs are compensated. HPF is a standard finite impulse response (FIR) filter performing the convolution in the time domain. Its cut-off frequency is at 60 kHz with transition width of 5 kHz. Next, the HPF samples are sent to the PLL block for compensating the short-term frequency drifts caused by DBSRX2 daughterboard, which can result in power misestimating.

PLL loop has been implemented by the GNURadio block "pll carrier tracking". The block mixes a received signal with its carrier frequency and outputs a signal on baseband as shown in Figure 6. The bandwidth, minimum frequency and maximum frequency are required as input parameters. They were set to 5000 Hz, 197000 Hz and 210000 Hz, respectively. Since the parameters must be given in rad/samp they are converted by the following equation

$$x = \frac{2\pi f}{f_{samp}} \, [rad \, / \, samp] \qquad (1)$$

Minimum and maximum frequencies are set with respect to the beacon signal frequency.

The PLL output signal in a baseband is passed to the stream-to-vector block where the stream of complex samples is transformed into a stream of complex vector of 65536 elements. The vector is passed on to a
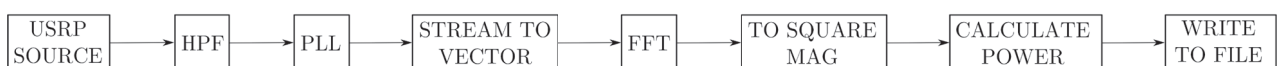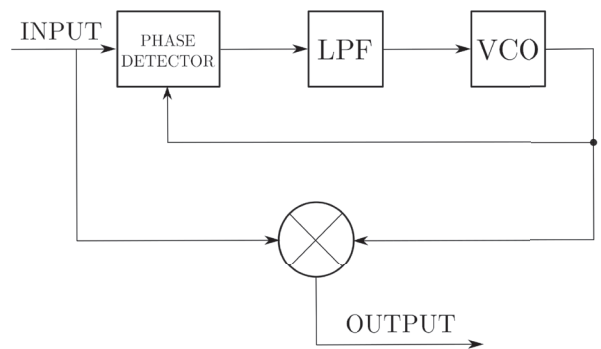


**Figure 6:** GNU Radio Phase-locked loop module block diagram
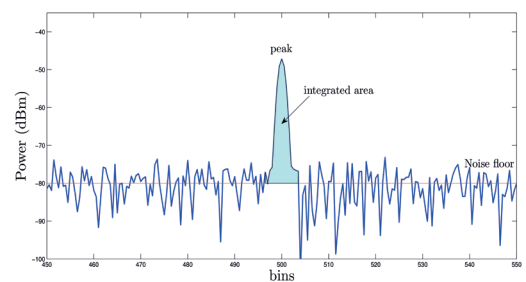


**Figure 7:** GNU Radio power calculation module [25]

block where FFT calculation is performed. Hanning window is used to reduce spectral leakage. The stream of complex spectrums is further sent to "mag squared block" which outputs a vector of squared spectral components magnitudes as real numbers. In the next step power estimation block takes a vector representing the signal's power spectrum, finds the signal and computes the power. Power calculation is performed by coherently adding the samples left and right of the spectrum's maximum, as shown in Figure 7. Therefore, output of this block is a real number which is written to a text file, along with a time stamp.

## 3 Receiver validation tests

In the development phase the receiver noise Figure has to be calculated, calibration of the receiver parameters must be performed, the dynamic range of the system has to be determined, measurement results have to be compared with parallel rain intensity measurements and scintillation characteristics must be estimated.



**Figure 5:** SDR signal processing block scheme [25]

### 3.1 Noise figure

The ADCs used in USRP N210 are ADS62P45 from Texas Instruments. The specified SNR is 73.8 dB and the maximum range is 2 $V_{pp}$ on 50 Ω input which gives $P_{max}$ = +10 dBm. Thus, the noise floor is calculated as

$$P_{nf} = P_{max} + SNR + ProcessGain \qquad (2)$$

In our case, vector size for FFT computation and power estimation is 65536 elements, which gives

$$10\log\left(\frac{N}{2}\right) = 45.15\,dB$$

$$(3)$$

of process gain. Therefore, the noise floor is

$$P_{nf} = +10dBm - 73.8dB - 45.15dB = -109dBm. \qquad (4)$$

The quantities described above are schematically illustrated in Figure 8. The MAX2112 chip on DBSRX2 has adjustable gain and it was set to 50 dB. Along with 22 dB gain provided by the LNA (MGA62563) allows reaching a full scale range on the AD converter at clear sky conditions. The received signal to noise ratio (SNR) is degraded by the receiver parts. Total noise temperature of the receiver is expressed as

$$T = T_A + T_{LNB} + \frac{T_C}{G_{LNB}} + \frac{T_{DBSRX2}}{G_{LNB}G_C} \qquad (5)$$

where the noise temperatures of the antenna $T_A$ and LNB $T_{LNB}$ are 94.7 K and 101.2 K, respectively, while the noise temperatures of the cable $T_C$ and dautherboard $T_{DBSRX2}$ are 290 K and 627 K. Note that the noise temperature values are taken from the elements' datasheets and can vary from their actual values. The gains of the LNB $G_{LNB}$ and cable Gc are 55 dB and -3 dB, corre-
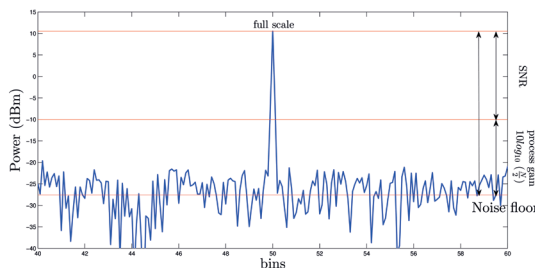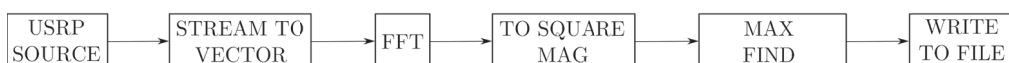
spondingly. The gain of the dautherboard $G_{DBSRX2}$ is set to 50 dB. Therefore, the total noise temperature of the system is 196 K which gives, according to the receiver noise figure expressed as

$$NoiseFigure(dB) = 10 * log10\left(\frac{T(K)}{T_{ref}(K)} + 1\right) \qquad (6)$$

where Tref = 290K, the total receiver noise figure of 2.24 dB.

### 3.2 Linearity test with dynamic range determination

The linearity and dynamic range of the USRP and daughterboard were verified by two test measurements.

In the first test the signal generator, generating continuous wave, was connected to the USRP with DBSRX2 daughterboard. Signal power was decreased from -50dBm to -130dBm in 1dB steps. The software flow graph used for this test is depicted in Figure 5 and the results are plotted in Figure 9. The results show satisfactory performance for the type of measurement that receiver is intended to perform.
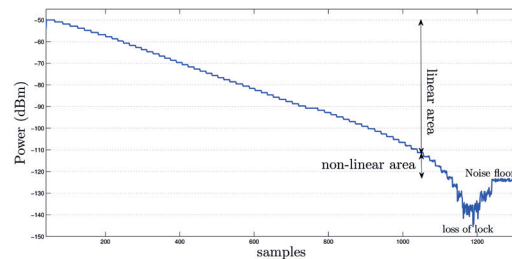


**Figure 9:** Linearity test with PLL block and high pass filter

During the second test the USRP with DBSRX2 daughterboard (with gain set to 50 dB) was connected to signal generator generating a continuous wave. Signal power was decreased from -50dBm to -130dBm in 1dB steps. The block scheme used for this test is depicted in Figure 10, note that the signal processing chain is without PLL processing block.

The plot of the results is presented in Figure 11. As it is seen, in this configuration the receiver is able to trace the range of around 60 dB. The result is obviously better than the previous; however, the problem is that this configuration cannot be used in real operation of the



**Figure 8:** Noise floor limit [25]



**Figure 10:** Linearity test block scheme [25]

receiver, due to unstable frequency reference in the MAX2112 tuner on the DBSRX2 daughterboard. We decided to circumvent this problem by designing our own additional down-conversion stage and then using the BasicRX daughterboard.
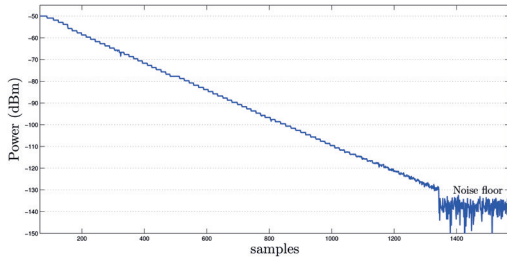


**Figure 11:** Linearity test without PLL block and high pass filter [25]

### 3.3 Receiver parameters calibration

For the purpose of optimal parameter settings, tests with waveguide attenuators and long-term frequency drift estimations were applied. In order to accurately determine dynamic range, waveguide attenuators were used. The attenuators have been placed in-between the LNB and the feed, as shown in Figure 12.



**Figure 12:** Waveguide attenuators for dynamic range determination

The experiment was started with full attenuator conductivity and typical receiver settings. Afterwards, the variations to various receiver parameters were applied and the attenuation was slowly increased until the signal was lost, thus checking the obtained dynamic range of new parameter settings. The experiment was repeated several times, applying variations to the number of FFT bins, sampling frequency, PLL bandwidth and gain. As a result of this test, we set values for the number of FFT bins to 65536 and the sampling frequency to 400 Hz. The frequency drift was causing occasional traverse of the carrier frequency out of the bandwidth borders, determined by the sampling frequency. To avoid occasional instability in received signal strength the PLL bandwidth value was set 5 kHz and minimum and maximum locking frequencies to 197 kHz and

210 kHz, respectively. However, to avoid this problem in the future, a routine for keeping the track of the carrier frequency was added.

### 3.4 Comparison with parallel rain intensity measurements at a nearby site

The main purpose of the designed receiver is to detect the atmospheric attenuation of the received beacon signal that is caused mainly by rain. Therefore, the measurements were compared with the rainfall intensity measurements made in parallel at a nearby site by a meteorological research group [13]. The measurements are recorded by a tipping-bucket rain gauge, which is about 170 m away from our station [14]. The resolution of the rainfall intensity measurements is 5 minutes. The two observed data sets are highly correlated, as seen in the example measurement day, 21st May 2012, shown in Figure 13.
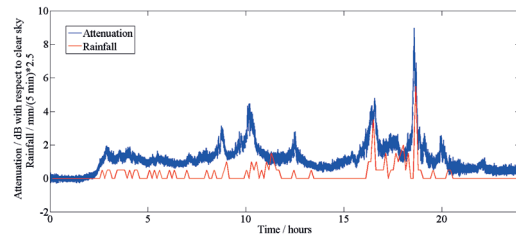


**Figure 13:** Comparison of attenuation time series with rainfall measurements on May 21, 2012

### 3.5 Estimation of scintillation characteristics

Data from a newly set up receiver were analysed by observing fast-fading events such as amplitude scintillation. The sampling rate performed by our receiver is sufficient for the study of scintillation characteristics.

We have written two procedures for scintillation analysis. The first procedure calculates the power spectral density of the signal in order to compare it with expected signal behaviour. The power spectral density of
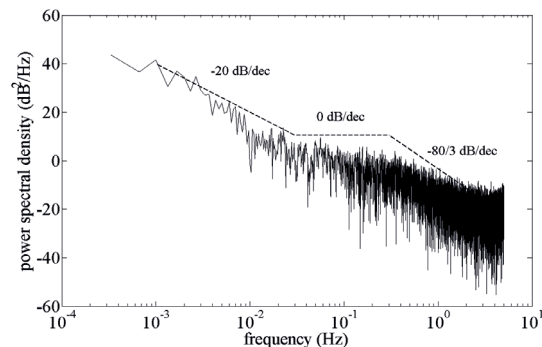


**Figure 14:** The measured signal spectrum on 24th May 2012 (solid line) compared to the theoretical model (dashed line)

scintillation can be described typically by a -20 dB/dec slope followed by a flat region and another slope with -80/3 dB/dec [15]. The theoretical spectrum is seen to agree well with the measurements. An example comparison for the measurements performed on a typical rainy day on 24th May 2012 is shown in Figure 14.

The second procedure was used to evaluate the long-term scintillation behaviour by comparison of cumulative distribution functions of measurements and existing scintillation models. The ITU-R P.618 [16] model provides a complementary cumulative distribution function (CCDF) of fade depth, based on long-term averages of atmospheric parameters and communication link characteristics. For our needs, the wet term of surface refractivity, which is one of the inputs to ITU-R P.618, has been expressed with the ITU-R P.453 model [17]. The modelled CDF has been compared to the measurements obtained in the time interval 24th May – 8th June 2012. In order to separate the scintillation phenomenon from the long-term attenuation variations, the measured signal has been filtered with a high pass filter with a cut-off frequency of 0.025 Hz [18]. The results in Figure 15 confirm receiver adequacy for scintillation detection.
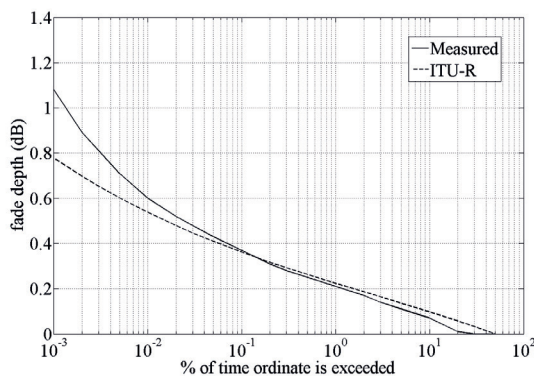


**Figure 15:** Complementary cumulative distribution function of the measured scintillation fade depth compared to the ITU-R model

## 4 Data processing procedure

The data obtained from the receiver are processed in 3 phases, where each phase represents a conversion from one data format to another. After each phase, a new intermediate result is obtained and saved in files. The last phase returns statistical results presented graphically. Figure 16 illustrates the whole process [19].
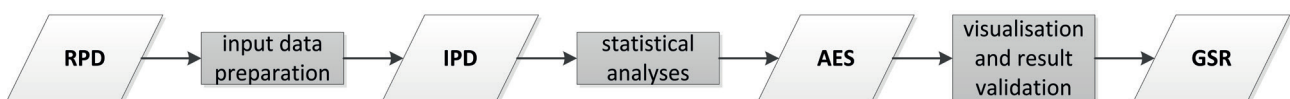
In the data processing tool, four data types exist and are processed in three data processing phases, namely:
- Raw Propagation Data (RPD),
- Intermediate Propagation data (IPD),
- Analysed Experimental Statistics (AES),
- Graphical Statistical Representation (GSR).

### 4.1 Data processing phases

The presentation of propagation experiment is performed in three different phases. In the *input data preparation phase (RPD – IPD)* the measured data is read, spikes are detected and operations which require interactions with the user (visually inspect signals and perform template extraction and calculate co-polar in-excess attenuation time series) are performed. The *statistical analyses phase (IPD – AES)* calculates complementary cumulative distribution functions (CCDF) of attenuation from a series of processed data, calculates second order distributions, i.e. fade slope and fade duration, and write the results in text files. In the last *visualisation and result validation phase (AES – GSR)* the visualisation of the obtained results as plotted graphs is performed and the results are compared to ITU-R models results.

The main tasks, performed in the *input data preparation phase* are spike detection, visual inspection and template extraction. In the beacon signal measurements, samples with obvious deviation from local average, so-called outliers or spikes, may occur. Their detection is performed automatically and they are flagged as doubtful. The method for spike detection is based on 2 min moving average based standard deviation, which is calculated continuously by:

$$\varepsilon(i) = \sqrt{\langle CPL(i)\rangle^2 - \langle CPL(i)\rangle^2} \qquad (7)$$

where the *CPL(i)* is the i-th beacon level sample within the day (dB) and $\langle CPL(i)\rangle$ mean value of *CPL(i)* using 2 minutes moving average filter (dB). The standard deviation serves as a threshold for comparison with actual samples. When the difference between the signal strength and its moving average $|CPL(i) - \langle CPL(i)\rangle|$ is larger than the threshold, defined as standard deviation, multiplied by a selected value *thresh_scale*, the sample is recognized as an outlier. Formally expressed, outliers are samples, for which the following equation holds:



**Figure 16:** Data processing procedure steps

$$\left| CPL(i) - \langle CPL(i) \rangle \right| > 5 \sqrt{\langle CPL(i)^2 \rangle - \langle CPL(i) \rangle^2} \qquad (8)$$

The operation is illustrated in Figure 17 with selected value *thresh_scale* = 5. The detected outliers are marked by red circles.
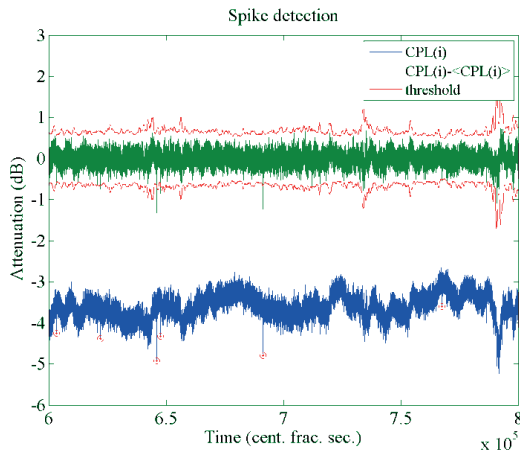


**Figure 17:** Spike detection example - spikes are marked by red circles

In order to assure correctness of automatically determined validity flags the measured values of beacon signal level are inspected visually on a daily basis. In case of irregular signal behaviour (saturation, fluctuation, missing samples, etc), the observed time frame is selected, its validity flags are changed from valid to invalid and samples are excluded from further analysis. Figure 18 (a) shows an example of regular behaviour of measured signal, where no actions are necessary while the signal shown in Figure 18 (b) is highly attenuated and reached saturation. In this case marked samples were excluded from statistical analysis.

Since the radiometer measurements are not available, the template extraction has to be used as a method for 0 dB level estimation. The procedure finds a function which corresponds to system-dependent received signal variations, and subtracts it from the beacon signal level. The purpose of this step is to eliminate all potential systematic errors, which deteriorate accurate evaluation of atmospheric impairments. Example sources of such errors are pointing errors due to satellite movements, gain instabilities in RF chains and other phenomena such as the wet antenna effect. While it is impossible to guarantee exactness of such a procedure, it is estimated that the systematic error is limited within a margin of maximum 1 dB. Experimental evaluation of the described effects has been performed in [4]. At the end of the procedure, the resulting signal corresponds to a sum of background attenuation in clear sky conditions and recorded atmospheric impairments.
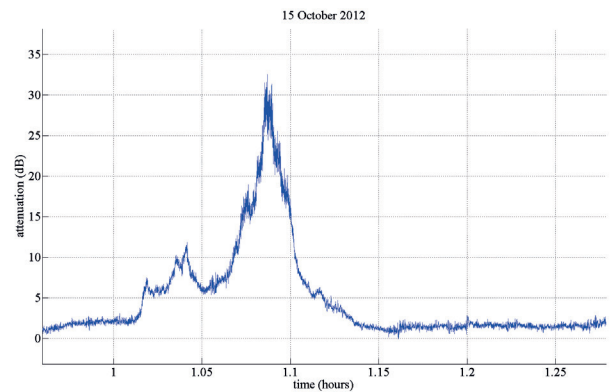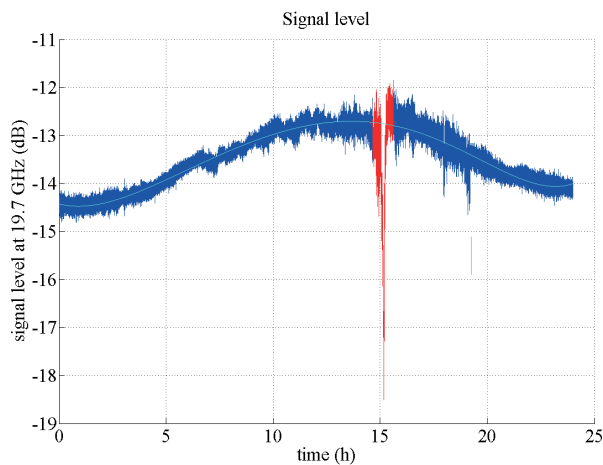


a)
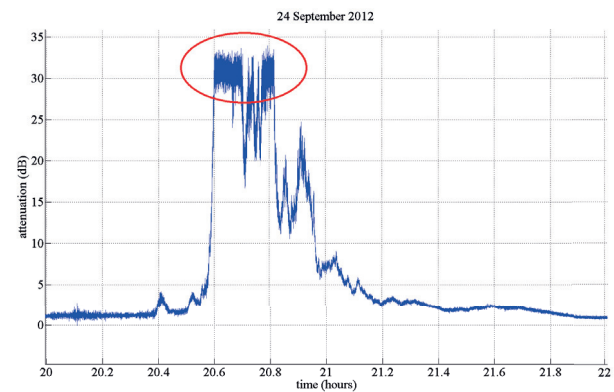


b)

**Figure 18:** Regular deep fade with no saturation (a) and with saturation (b)

The search for template function represents finding a moving average of the received beacon signal in clear sky conditions and finding of a proper interpolation for the time intervals with rain events. The procedure is divided into three steps: (i) determination of events, (ii) finding template function, (iii) subtraction.
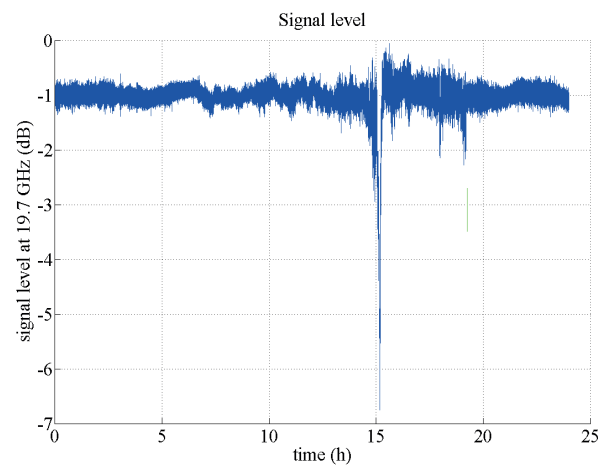
In the first step, the events with strong fluctuations are identified and flagged. The second step depends on the form of the beacon signal (i.e. clear sky with no oscillations, rain event presence and oscillating signal) which dictates the selection of the adequate method (i.e. maximum probable value detection, polynomial fitting and FFT based interpolation). Maximum probable value detection sorts detected signal levels according to their frequency of appearing. The most frequent value is selected. In polynomial fitting, a polynomial function of a selected order is found to fit the measured beacon signal. In FFT based interpolation, a Fast Fourier Transform is used for this purpose, and is especially suitable for oscillating signals with periodic behaviour. In practice, the polynomial fitting method is mostly used. Finally, in the last step, the obtained template function is subtracted from original beacon signal.

Figure 19 depicts an example template extraction for the measurements, obtained on the day with rain event. In the first step, an interval not to be considered is chosen (Figure 19 a, red colour) while in the second step, a polynomial function of 6th order is determined according to remaining beacon signal (Figure 19 a, cyan line). The obtained signal is shown in Figure 19 (b). In this example, the mispointing error due to the inclined orbit of the satellite may be clearly observed as a periodic signal fluctuation. If the polynomial fitting was not applied, a systematic error of about 2 dB would have been added. It is clearly seen how the procedure eliminates the error, such that the clear-sky levels are correctly represented, while the rain-induced attenuation remains.

The task of the *statistical analyses phase* is to calculate statistics from the obtained attenuation time series. In this phase the co-polar attenuation analysis, fade duration analysis and fade slope analysis are performed. Co-polar attenuation analyses include reading the long term attenuation data and calculating their complementary cumu-
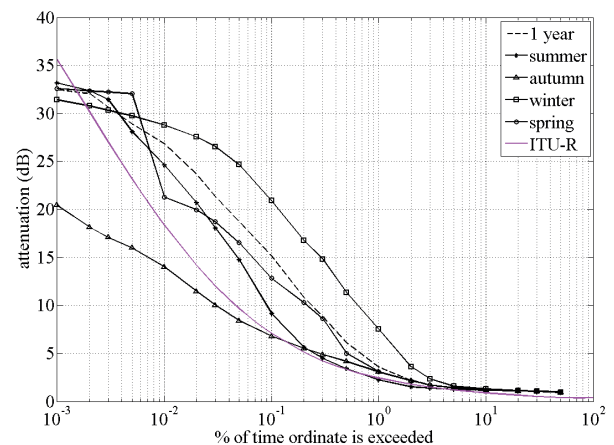
lative distribution function (CCDF). For the fade duration analysis long term attenuation data are read and relative number of event CCDF and relative fade time CCDF are calculated. Fade slope statistics are calculated by determination of signal dynamics (derivative) and their expression in terms of cumulative distributions.
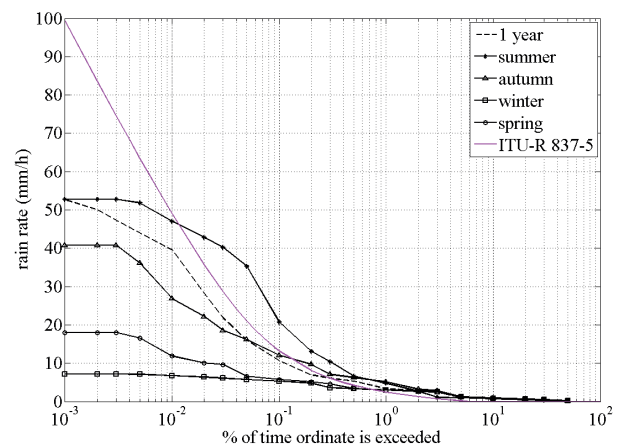
In the final phase, *visualisation and result validation phase,* the statistical analyses results, namely CCDF of attenuation, CCDF of relative number of fades, CCDF of relative fade times and CCDF of measured fade slopes, are graphically presented.

## 5 Analyses of the measurement results

In this section, the results are presented for one full year of analysed data. In addition to attenuation analysis, also the rain rate analyses for the same time period have been performed. The complementary cumulative distribution functions (CCDF) have been calculated for various time scales, i.e. for 1 full year and for 4 different



a)



b)

**Figure 19:** Determination of event and the template function (a), resulting signal (b)



a)



b)

**Figure 20:** CCDF of attenuation (a) and CDF of rain rate (b)

seasons (summer, autumn, winter, spring). The results are depicted in Figure 20. In Figure 20 a, the cumulative distribution functions of attenuation are given in comparison to ITU-R P.618 model [16], while graph in Figure 20 b, depict cumulative distribution functions of rain rate compared to the ITU-R 837-5 model [20].

In general, the results comply well with expectations, both in terms of comparison to the ITU-R models as well as in terms of seasonal variations (more severe rain and consequently attenuation in summer months) for low probabilities. The comparison of attenuation distributions with rain rate distributions also reveals similarities, especially for autumn and summer months.

However, in winter and spring there are some deviations, which are due to the snow. While the rain gauge cannot correctly measure the snow quantities, the snow still affects the received signal strength, which may be even further deteriorated if snow sticks to the satellite dish. Although the snow from the dish was cleaned regularly and the measurements with obvious deviations were discarded later, the effect could not be completely eliminated.

Second order statistics analysis has been made for the same time period as for the attenuation statistics. Fade duration is defined as the time interval between two crossings above the chosen attenuation threshold, while the fade slope represents the rate of change of attenuation with time. Both for the fade duration and fade slope statistics, a filter with cut-off frequency 25 mHz has been applied. For the fade slope calculations, the time interval to consider was set to 2 s. The ITU-R P.1623-1 model [21], proposed by Van de Kamp [22], has been used for comparison.

The fade slope statistics are depicted in Figure 21. The distributions for 5 dB attenuation level match quite well the model. For the other chosen attenuation lev-
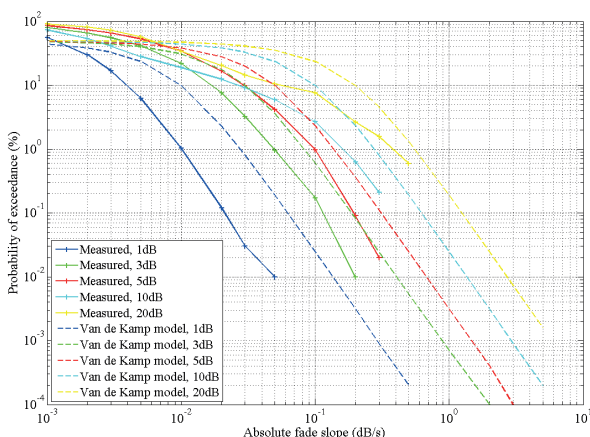
els, a slight deviation may be observed, similarly as in some other studies [23], [24].

The fade duration distributions in Figure 22 show some discrepancy between the measured values and the model, but the trend is similar. Also variations due to differently chosen attenuation thresholds follow similar rules. For lower thresholds, the relative number of fades and relative fade times are proportionally higher.
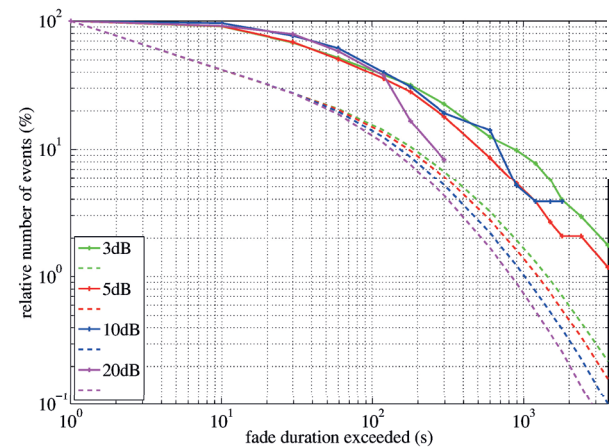


a)
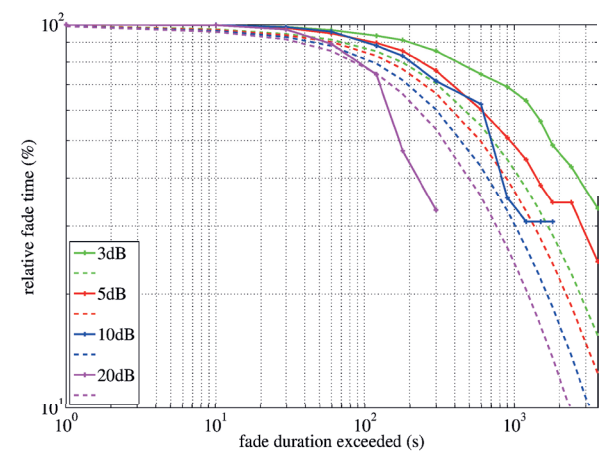


b)

**Figure 22:** CCDF of measured relative number of fades (a, solid lines) and relative fade times exceeding given fade durations (b, solid lines) in comparison to ITU-R P.1623 model (dashed lines)

## 6 Conclusion

The low-cost SDR beacon receiver passed all tests successfully, confirming that we established a reliable measuring system. In general we confirmed that the obtained results comply well with expectations, both in terms of comparison to the ITU-R models as well as in terms of seasonal variations.



**Figure 21:** CCDF of measured fade slopes in comparison to Van de Kamp model

Although focusing on the beacon measurements in Slovenia, the project results are important and interesting also for the broader satellite communications research community. On the European scale, we contributed with the project to the ESA scientific experiment which aims at a coordinated acquisition of propagation measurements in Europe.

## 7 Acknowledgement

## 8 References

1. R. K. Crane, "Propagation Handbook for Wireless Communication System Design", CRC Press, 1st edition, 2003.
2. X. Boulanger, G. Carrie, L. Castanet, L. Casadebaig, B. Gabard, "Statistics of Total Attenuation and Fade Dynamics From Measurements in Toulouse of the 19.7 GHz Beacon of Eutelsat Hot Bird 6," In Proc. 6th European Conf. Ant. and Prop. (EuCap), pp.81-85, 26-30 March 2012.
3. L. E. Braten, J. Sander and T. Mjelde, "Satellite-Earth K-band Beacon Measurements at Kjeller, Norway; Measurement setup and initial results," In Proc. 7th European Conf. Ant. and Prop. (EuCap), pp.47-51, 8-12 April 2013.
4. Teschl F., F. Cuervo, A. Martellucci, J. Rivera Castro, . Riva, G. Codispoti, K. Plimon, M. Schönhuber, "The Ka/Q-band Alphasat Ground Propagation Terminal – First Months of Operation", The 8th European Conference on Antennas and Propagation (EuCAP 2014), The Hague, The Netherlands, April 6-11, 2014,
5. C. J. Kikkert and O. P. Kenny, "A digital signal processing based Ka band satellite beacon receiver," In Proc. IEEE Int. Conf. Electronics, Circuits and Systems, pp. 598-601, Aug. 31. Sept. 3, 2008.
6. A. C. D. Rocha, R. Sousa, A. Pires, R. Martins, "PLL based detector for coherent beacon receivers using DSP techniques," ISCCSP 2008, Malta, 12-14 March 2008, pp. 1576 - 1579.
7. M. Cheffena and L. E. Br°aten, "Low-Cost Digital Beacon Receiver Based on Software-Defined Radio," IEEE Antennas and Propagation Magazine, vol.53, no.1, pp.50-55, 2011.
8. Riva C., L. Castanet, L. Csurgai-Horvath, O. Fiser. F. Lacoste, F.S. Marzano, F. Perez Fontan, J.M. Riera, A. Rocha, M. Schönhuber, A. Vilhar, "The Aldo Paraboni scientific experiment: the preparation and plans for an European measurement campaign", The 20th Ka and BroadBand Communications, Navigation and Earth Observation Conference, Vietri, Italy, October 1-3, 2014, pp. 367-375
9. Prodelin Ka-band antenna technical data, webpage: http://satcomnow.com/satcom/pdf/ Prodelin_3120.pdf.
10. Norsat Low Noise Block technical data, webpage: http://www.norsat.com/wp-content/uploads/9000h_lnb1.pdf.
11. Ettus, webpage: http://www.ettus.com/
12. Gnu Radio, webpage: gnuradio.org/.
13. G. Skok, T. Vrhovec: "Considerations for interpolating rain gauge precipitation onto a regular grid", Meteorologische Zeitschrift, vol.15, no. 5, pp.545-550, 2006.
14. Vaisala rain gauge RG13 specifications, http://www.vaisala.com/en/meteorology/products/
15. E. Matricciani, M. Mauri, and C. Riva: "Scintillation and simultaneous rain attenuation at 12.5 GHz to satellite Olympus", Radio Science, vol.32, no.5, pp.1861–1866, 1997.
16. ITU-R P.618-10: "Propagation data and predition methods required for the design of earth-space telecommunication systems", Geneva, ITU, 2007.
17. ITU-R P.453-9: "The radio refractive index: its formula and refractivity data", Geneva, ITU, 2003.
18. E. Matricciani, M. Mauri, and C. Riva: "Relationship between scintillation and rain attenuation at 19.77 GHz", Radio Science, vol.31, no.2, pp.273–279, 1996.
19. A.Vilhar: Data processing and channel modelling for propagation experiments at Ku/Ka/Q/V-bands, Technical report, DEMR-ONERA, October 2010.
20. ITU-R Recommendation P.837-5, "Characteristics of precipitation for propagation modelling," International Telecommunication Union, Geneva, Switzerland, 2007.
21. ITU-R Recommendation P.1623-1, "Prediction method of fade dynamics on Earth-space paths," International Telecommunication Union, Geneva, Switzerland, 2005.
22. Max M.J.L. van de Kamp, "Statistical Analysis of Rain Fade Slope", IEEE Transactions on Antennas and Propagations, vol. 51, no. 8, pp. 1750-1759, 2003.
23. H. Dao, M.R. Islam, K. Al-Khateeb, "Modification of ITU-R Rain Fade Slope Prediction Model Based on Satellite Data Measured at High Elevation Angle", IIUM Engineering Journal (IIUMEJ), vol. 12, no.8, pp. 53-59, 2011.
24. R. Singliar, B. Heder and J. Bito, "Rain Fade Slope Analysis", Broad-Band Europe, Bordeaux, France, 12 - 14 December 2005.
25. A. Vilhar, U. Kuhar, A. Hrovat, G. Kandus, "Ka/Q-band propagation measurements and modelling for the design of prediction and impairment mitigation techniques (SatProSi): technical report", (IJS delovno poročilo, 12025, zaupno), 2014.